*Physics – Uspekhi* **68** (4) 401 – 407 (2025) 

*INSTRUMENTS AND METHODS OF INVESTIGATION* PACS numbers: **68.37. – d,** 68.37.Hk

ON THE 270th ANNIVERSARY OF M.V. LOMONOSOV MOSCOW STATE UNIVERSITY (MSU)

# Effect of increasing the coefficient of backscattered electrons for multilayer nanostructures and image contrast inversion in scanning electron microscopy

E.I. Rau, S.V. Zaitsev

DOI: https://doi.org/10.3367/UFNe.2025.01.039838

## Contents



**Abstract. We discuss the reasons for an increase in the coefficient of backscattered electrons (BSEs) for multilayer film nanostructures during their study with a scanning electron microscope (SEM) and consider the conditions for the occurrence of contrast inversion of their images. A complete analytical expression for the signal detected in the BSE regime by an SEM is derived for the first time for multilayer nanostructures. Solving direct and inverse problems relating the signal values to the composition of a three-dimensional sample as a function of the energy of probe electrons allows the thicknesses and depths of nano-objects to be determined in a matrix array with high spatial resolution. The main calculations in this paper are performed using refined empirical formulas corresponding to the experimental data obtained by the authors or presented in the cited literature.**

**Keywords:** scanning electron microscopy, backscattered electrons, multilayer thin-film structures, image contrast

## 1. Introduction

With the rapid development of nanotechnology in recent decades, scanning electron microscopy has become increasingly popular as a versatile tool for monitoring and diagnosing three-dimensional nanostructures.

**E.I. Rau** (*), **S.V. Zaitsev** (**)
Lomonosov Moscow State University, Faculty of Physics,
Leninskie gory 1, str. 2, 119991 Moscow, Russian Federation
E-mail: (*) rau@phys.msu.ru, (**) zai336@mail.ru

Received 7 June 2024, revised 5 December 2024
*Uspekhi Fizicheskikh Nauk* **195** (4) 425 – 431 (2025)
Translated by I.A. Ulitkin

This is facilitated by such advantages of scanning electron microscopes (SEMs) as high spatial resolution (up to units of nanometers) and a large information depth equal, in order of magnitude, to that of primary electrons in a massive target (up to units of micrometers at primary electron energies of tens of keV) [1, 2]. A wide range of detectable signals, for example, in the regimes of secondary electron emission, backscattered electrons (BSEs), X-ray spectral microanalysis, cathodoluminescence, and electron-induced current makes SEMs indispensable and powerful instruments for obtaining unique information about structure, composition, and properties of new materials and devices.

One of the priority tasks in the nanotechnology industry, including in the field of micro- and nanoelectronics, is the study and quality control of submicron multilayer devices, in particular, the determination of the thickness of local nanofilms on massive substrates. In general, this problem has been solved quite successfully using BSE signal detection in an SEM [3–6], but only as applied to one film on a substrate. The advantage of this method is that it allows, along with visualization of the object, the local thicknesses of optically opaque films to be nondestructively determined with submicron lateral resolution.

Afanas'ev et al. [7] and Mikheev [8] made a significant contribution to the solution of the direct and inverse problems of analyzing the BSE signal from film structures. Consistent improvement of the methods and refinement of the calculation formulas for determining the thickness of films on substrates in an SEM was performed in papers [9–11].

As for the measurements of thicknesses and depths of individual near-surface details, for example, subsurface local films in multilayer structures, only a few papers have been published so far [12–16]. The solution of both the direct and inverse problems is much more complicated than that in the case of the above-considered 'film-on-substrate' structure.

In this paper, the stated problems are solved completely for the first time and the corresponding relationships between the value of the detected signal and the parameters of the three-dimensional nanostructure are derived. In this case, use is made of the calculation algorithm and the refined formulas proposed in [14] and [15], respectively. Of certain interest and practical significance is also the phenomenon of contrast inversion of images of multilayer nanostructures. Contrast inversion in an SEM in the BSE detection regime has attracted attention for quite a long time [17–21], but until now there has been no complete explanation of its occurrence. Thus, in their earlier papers, Aristov et al. [17, 18] did not present any analytical expressions for the $I_S$ signal, except for the data of experimental measurements, and did not discuss the role of the hardware function of the BSE detectors. On the contrary, Hejna [19] assumed that the geometry of the experiment and the hardware function play a major role in the appearance of the contrast inversion of images of multilayer thin-film structures. Kowoll et al. [21] used Monte Carlo calculations of the signal to explain the inversion; however, their paper lacked visual physical and mathematical description and calculation formulas for the $I_S$ signal, without which it is difficult to interpret the results. In the present paper, due attention is paid to this problem, and correct calculations of the image contrast are performed, in good agreement with the experiments.

Another method in this field of research can be nanotomography in X-ray imaging. The method is implemented either in an SEM [22] or in installations using focused synchrotron radiation [23]. In the latter case, the spatial resolution is comparable to that in the BSE detection regime using an SEM. However, the main limitation is that only a few large research centers equipped with a synchrotron radiation source are capable of implementing this regime. With phase-contrast imaging, when traversing the sample, the substrate must be thinned, while an SEM makes it possible to study, for example, multi-level integrated circuits in a housing with the top cover removed. This circumstance can be significant in flaw detection and failure analysis of microelectronic products. The X-ray standing-wave technique [24, 25] also allows one to obtain quantitative characteristics of three-dimensional nanostructures, but it is not widely used, since it requires specialized laboratory facilities. Unlike X-ray methods, the technique proposed in this paper is generally available and can be implemented using widely used serial devices such as SEMs.

## 2. Detection of the effect of increasing the coefficient of backscattered electrons for film multilayer nanostructures

The experiments were performed using LEO1455 (Zeiss, Germany) and Quanta (FEI, USA, Netherlands) SEMs with commercial standard silicon detectors.

The object of the study was a layered structure of nanofilms with calibrated thicknesses. Figure 1 shows the drawing of the nanostructure. It consists of a massive silicon substrate *5*, onto which two gold films (thicknesses $d_1 = 10.8$ nm and $d_2 = 19.9$ nm) are deposited by thermal evaporation (sections *1* and *2*). The size of each film is $200 \times 100$ μm$^2$. The structure top is partly covered with a 150-nm-thick aluminum film measuring $200 \times 100$ μm$^2$. The aluminum film covers only a quarter of each gold film (sections *3* and *4*). The images of this layered nanostructure

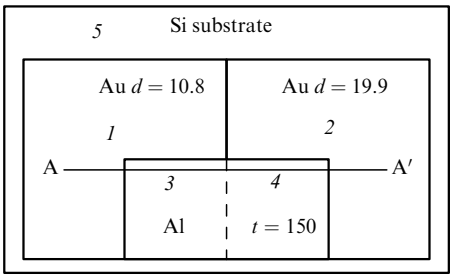


**Figure 1.** Structure consisting of a Si substrate (section *5*) with deposited Au films of thickness $d = 10.8$ nm (sections *1* and *3*) and $d = 19.9$ nm (sections *2* and *4*). Sections *3* and *4* are covered from above with an Al film of thickness $t = 150$ nm and a size of $200 \times 100$ μm.

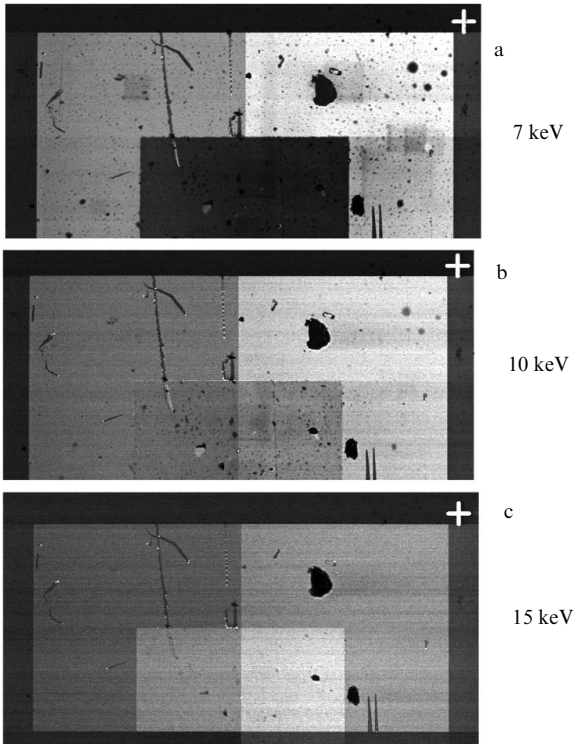


**Figure 2.** Images of the multilayer nanostructure shown in Fig. 1 during BSE detection using an SEM. The images are obtained at different energies $E_B$ of the irradiating electrons.

obtained at three energies of primary irradiating electrons in the SEM detection regime are shown in Fig. 2.

These images show a phenomenon that is surprising at first glance: at certain energies $E_B$, the images of the sections of the Au films hidden under the aluminum film become brighter than those of the open Au films on the silicon substrate. Thus, in Fig. 2a at $E_B = 7.0$ keV, the uncovered sections of the Au films look light, while the square section covered by the Al film looks dark, and the images of the sections with Au under this film are invisible. At $E_B = 10$ keV, the near-surface sections of the Au films become visible, the contrast of the images of the closed and open sections of the Au films is almost the same, and the image of the Al film disappears (Fig. 2b). Finally, at $E_B = 15$ keV, a striking phenomenon is observed: the image of the buried sections of the Au films, previously invisible, becomes brighter than that of the open sections (Fig. 2c). The question arises: Does such an increase in the $I_S$ signal result from an increase in the BSE coefficient in the

corresponding sections of the structure and, if so, what are the reasons for this?

## 3. Calculation of the $I_S$ signal from semiconductor detectors for multilayer film nanostructures

The BSE current from semiconductor detectors, $I_S$, is generally represented by the expression [1]:

$$I_S = I_B \eta_{sf} \left( \frac{E_{sf}}{E_i} \right) f(\Omega) \left[ (1 - \eta_D) \left( 1 - \frac{E_{th}}{\varepsilon_{sf} E_{sf}} \right) \right], \qquad (1)$$

where $\eta_s$ is the coefficient of BSEs from the sample, $E_s = \varepsilon_s E_B$ is the average BSE energy with the coefficient $\varepsilon$, $E_i$ is the energy of generation of an electron–hole pair in the detector material, $\Omega$ is the solid angle of collection of BSEs by this detector, $\eta_D = f(E_s)$ is the coefficient of BSEs from the detector, $E_{th}$ is the threshold energy of the detector at which $I_S = 0$, and $\theta$ is the average angle of reflection of electrons.

The experimental technique is based on the principle of calibrating this signal using the gray-level scale of the microscope screen [26–28]. If the composition of the sample is known, then the gradation of the gray-level scale from 0 to 1 is made using the minimum signal $I_{01}$ from the lightest element with atomic number $Z_1$ and the maximum signal $I_{02}$ from the heavy element with atomic number $Z_2$. These signals at one of the selected energies of primary electrons, $E_B$, are equal for the massive standard samples, i.e., samples $Z_1$ and $Z_2$:

$$I_{01} = \left[ L + C(\eta_1, \varepsilon_1) \right] F_1 ,$$
$$I_{02} = \left[ L + C(\eta_2, \varepsilon_2) \right] F_2 , \qquad (2)$$

where $\eta$, $\varepsilon$, and $F$ are, respectively, the BSE coefficient for materials $Z_1$ and $Z_2$, the coefficient of their reflected average energy, and the response function ($F$) of the detector. The massive standard samples are mounted on the stage together with the sample under study. If the chemical composition and structure of the sample are not initially known, then an X-ray spectral microanalysis of the sample is first carried out using an X-ray microanalyzer, which all modern SEMs are equipped with [13]. Thus, according to two equations (2), the constants of the microscope settings are determined: $L$ is the signal level and $C$ is the contrast (gain) of the signal from the sample. After determining $L$ and $C$ from the $I_S$ signals at two energies of primary electrons $E_{B1}$ and $E_{B2}$ (Fig. 3), it becomes possible to find the film thicknesses $d$ and $t$ [15].

The signals $I_{S1}$ and $I_{S2}$ are found from the experimental profiles of the linear scanning of the sample. Typical profilograms are shown in Fig. 3 for energies $E_B = 7$ and 15 keV. These profilograms, as well as the images in Fig. 2, demonstrate the effects of an anomalous increase in the signal and the inversion on the double layer with respect to a single layer on the substrate.

Coefficients $\eta$ are found using the following empirical relation proposed by us, which differs from those given in [29–31] by the values that are closer to the experimental [32–34] ones:

$$\eta_s(Z, E_B) = \exp(-6.4 Z^{-0.5}) \left[ \frac{1 + \ln(Z/33)^{0.5} (1 + 0.16 \ln E_B^{0.666})}{1 + \ln(Z/33)^{0.5} (1 + 0.16 \ln 10^{0.666})} \right], \qquad (3)$$

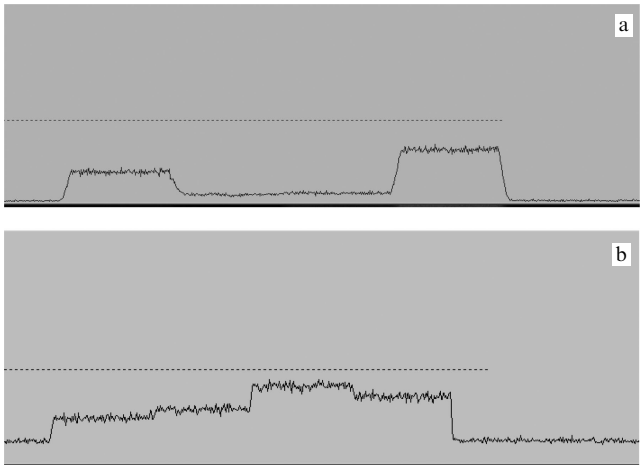


**Figure 3.** Signals $I_S$ recorded during linear scanning along the line A–A′ (Fig. 1) at an energy of $E_B = 7$ (a) and 15 keV (b).

where the energy $E_B$ is normalized to 1 keV, and the value of $E_B = 10$ keV is given in the denominator in square brackets. Formula (3) is valid for elements at $Z > 10$, while at $Z < 10$, the values of $(1 + 0.08 \ln E_B^{0.333})$ should be used in the numerator, and the value of $(1 + 0.08 \ln 10^{0.333})$ should be used in the denominator. The next parameter $\varepsilon_s$ in Eqns (1) and (2) is determined by a slightly more refined expression from [35]:

$$\varepsilon_s = \frac{E_s}{E_B} = 0.46(1 + 1.6\eta_s) . \qquad (4)$$

Finally, the detector response function when measuring the BSE spectrum from a sample is determined by the relation:

$$F = (1 - \eta_D) \left( 1 - \frac{E_{th}}{\varepsilon_s E_s} \right), \qquad (5)$$

where $E_{th} = 0.75/\varepsilon_s$ determines the average value of the threshold energy of the BSE detectors, and the value of 0.75 keV refers to the response to a monoenergetic electron beam (found by us experimentally). The value of the BSE coefficient of the detector material, $\eta_D$ (in this case, from a Si crystal), when the energy $E_s$ reflected from the sample is incident on it, is found from relation (3) for the silicon material by using the value of $E_S$ instead of $E_B$.

Let us describe the sequential calculation of the $I_S$ signal from the detector, illustrating it with specific examples. We will use the method proposed in [18] and schematically shown in Fig. 4.

Let us consider a fragment of the previously described sample (according to Figs 1 and 2). We will use a 10 nm thick Au film on a Si substrate (composite system $S_1$). Part of this structure (film on the substrate) is covered with an Al film with a thickness of $t = 150$ nm (system $S_2$).

To determine $I_S$ using formulas (1) and (2), it is necessary to calculate the coefficients $\eta$, $\varepsilon$, and $F$. The BSE coefficient $\eta_{sf}$ of the $S_1$ system (a film of thickness $d$ with atomic number $Z_f$ on a massive substrate with atomic number $Z_S$) is calculated using the well-known formula [3–5]:

$$\eta_{sf} = \eta_{os} + (\eta_{of} - \eta_{os}) \left( \frac{\eta_f}{\eta_{of}} \right), \qquad (6)$$

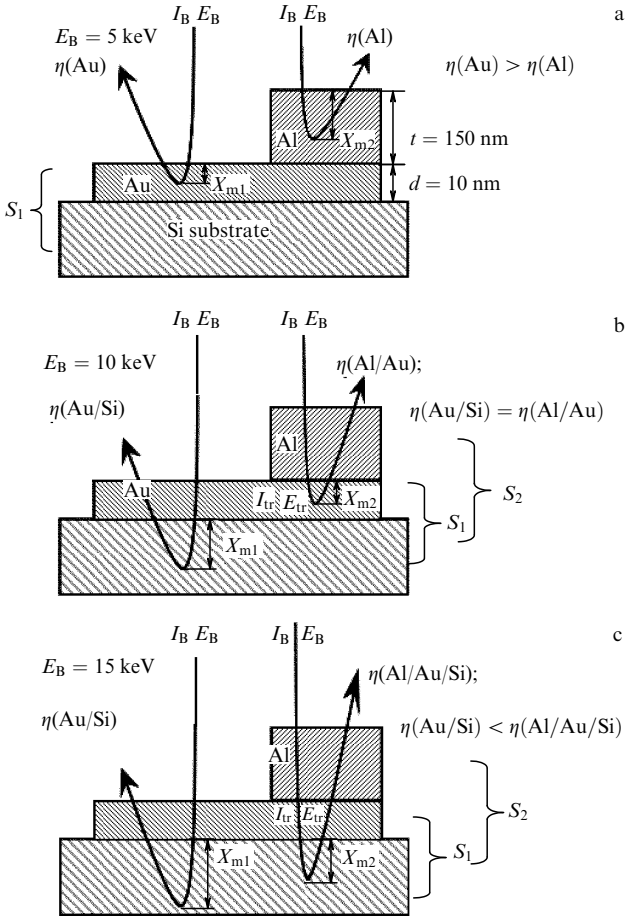


**Figure 4.** Scheme of interaction of a primary electron beam at current $I_B$ and energy $E_B$ with a two-layer Al–Au film structure located on a massive Si substrate.

where $\eta_{os}$ and $\eta_{of}$ are the coefficients of BSEs from the materials of the substrate with $Z_s$ and the massive film with $Z_f$. They are determined using formula (3). The relative coefficient of BSEs from a film of thickness $X$ is generally determined using the formula [35]:

$$\frac{\eta_f}{\eta_{of}} = 1 - \exp\left[-A\left(\frac{X}{R}\right)^P\right], \tag{7}$$

where $X$ is either $d_i$ (the thickness of the Au film on the Si substrate) or $t$ (the thickness of the upper Al film). The empirical expressions for the parameters $P$ and $A$ for different targets are as follows [15, 36]:

$$P = 1.11\eta^{-0.333}, \quad A^{-1} = \frac{X_m}{R} = 0.55\exp\left[-0.022(Z+3)\right], \tag{8}$$

where $X_m$ is the average depth of electron reflection in the sample. The electron path depths in the materials of the sample, $R$, and the detector, $R_D$, will be determined by the formula averaged over many publications (see, for example, [1]):

$$R = 67.5E^{1.5}\rho_m^{-0.85}, \tag{9}$$

where $R$ is given in nm, and the specific density target material $\rho_m$ is measured in g cm$^{-3}$.

Let us return to the qualitative consideration of Fig. 4. At $E_B = 5$ keV (Fig. 4a), we have $X_{m1} = 4.8$ nm on the Au film ($d = 10$ nm) and $X_{m2} = 119$ nm on the Al film ($t = 150$ nm). Thus, the electron probe is not able to pass through these films, which are massive targets in this situation. Here, $\eta(\text{Au}) \gg \eta(\text{Al})$; therefore, a strong contrast from the structure ($Z$ is the contrast) appears in the images. At $E_B = 10$ keV (Fig. 4b), the electron probe already penetrates both films, since $X_m(\text{Au}) = 13.5$ nm, and $X_m(\text{Al}) = 338$ nm. As a result, for two sections of the sample, as will be shown below in the calculations, we have almost equal signals $I_S$, since $\eta(\text{Au/Si}) \approx \eta(\text{Al/Au})$. And, finally, for the case of $E_B = 15$ keV (Fig. 4c), we have inverse values of the $I_S$ signal, since

$$\eta\,(\text{Au/Si}) < \eta\,(\text{Al/Au/Si})\,.$$

Now the electron probe penetrates the composite system $S_2$ and interacts with the complex system $S_1$. The sections located under the Al film are affected by the flux $I_{tr}E_{tr}$ weakened in intensity and energy rather than by the electron flux $I_BE_B$. The flux intensity $I_{tr}$ is characterized by the expression [35]:

$$\eta_{tr} = \left(1 - \eta_f(\text{Al})\right)\exp\left[-4.605\left(\frac{t}{R(\text{Al})}\right)^{1.98}\right], \tag{10}$$

where $\eta_f(\text{Al})$ is determined from (7), and $R(\text{Al})$ is found from (9).

The average energy loss for electrons passing through the Al film of thickness $t$ is determined by the expression [35, 36]:

$$\varepsilon_{tr} = \frac{E_{tr}}{E_B} = \alpha\exp\left[-\frac{t(\text{Al})}{R(\text{Al})}\right], \tag{11}$$

where $\alpha = 1 - \eta_f(\text{Al})$. An important remark should be made here, which consists in the fact that the energy $E_{tr}$ passed through the film of thickness $t$ has a distribution with the most probable value of $E_p$. This energy, according to the analysis of transmission spectra [1, 36–39], can be approximated by the empirical expression:

$$E_p = E_0\left[1 - 0.666\left(\cos\left(\arcsin\left(\varepsilon_{tr}\right)\right)\right)\right]. \tag{12}$$

This value is used for the energy incident on the $S_1$ system (Si substrate–Al film). Consequently, it is necessary to recalculate the parameters, in particular, the coefficients $\eta_0(\text{Si})$, $\eta_0(\text{Au})$, and $\eta_{sf}(\text{Au/Si})$ according to formulas (3), but with the substitution of $E_B$ by $E_p$. The second important consequence of the energy transformation is the change in the primary electron path depth in the Au film, which is calculated as before according to formula (9), but now at the energy $E_p$. Then, according to the above scenario of finding the values of $\eta_{sf}$, $\varepsilon_{sf}$, and $F_{sf}$ for the $S_1$ system, new values of $\eta'_{sf}$, $\varepsilon'_{sf}$, and $F'_{sf}$ are calculated, but already for the $S_2$ structure. Successive substitution of expressions for $\eta_{sf}$, $\varepsilon_{sf}$, and $F_{sf}$ in (1) yields the formula for the signal from the composite system $S_1$ (of thickness $d$ on a massive substrate):

$$I_{sf} = \beta[\eta_{sf} + 1.6\eta_{sf}^2]\left(1 - \eta_D(E_{sf})\right)\left[1 - \frac{E_{th}}{0.21E_B(1 + 1.6\eta_{sf})^2}\right],$$

where

$$\eta_{sf} = \eta_{os} + (\eta_{of} - \eta_{os})\left[1 - \exp\left(-A_d\left(\frac{d}{R_0}\right)^{P_1}\right)\right]. \quad (13)$$

Expression (13) is a transcendental function in which the value of $d$ is found by the iteration method or using computer programs. The following parameters are included in (13): $R_0$ is the electron path depth in Au,

$$\beta = \text{const} = \frac{I_B f(\Omega)}{E_i},$$

$$\eta_{os} = \eta_s(\text{Si}), \quad \eta_{of} = \eta_s(\text{Au}),$$

and the parameters $A_d$ and $P_1$ for Au are found from (8). The formula for the $I'_S$ signal from the $S_2$ system (a double layer of films on a substrate) is even more cumbersome, since it includes the term $\eta_{sf}$ as $\eta_{os}$ from equation (13), parameters $A_t$ (instead of $A_d$) and $P_2$ (instead of $P_1$) for the upper cover film Al, and new values of $\eta_s(E_p)$ and $R(E_p)$ determined from the above formulas. In this case, a new transcendental equation is also solved and the sought for parameters $d$ and $t$ are found by the iteration method.

Let us give as an example numerical estimates of the parameters $\eta_{sf}$ and $\eta'_{sf}$ as well as the signals $I_{sf}(\eta_{sf}, \varepsilon_{sf}, F_{sf})$ and $I'_{sf}(\eta'_{sf}, \varepsilon'_{sf}, F'_{sf})$ at $E_B = 15$ keV, $t(\text{Al}) = 150$ nm, $d(\text{Au}) = 10.8$ nm, and verify that $\eta'_{sf} > \eta_{sf}$ and $I'_{sf} > I_{sf}$. Thus, for the $S_2$ system, $\eta_{so}(\text{Au}) = 0.493$, $\eta_{so}(\text{Si}) = 0.174$, $\eta_{sf}(\text{Au/Si}) = 0.26$, $\varepsilon_{sf}(\text{Au/Si}) = 0.656$, $F(\text{Au/Si}) = 0.723$. Hence, the signal $I_S(\text{Au/Si}) = 0.64$, which coincides with the experimentally measured value with an error of 2.5%. Below, for the $S_2$ structure, i.e., for a double layer of dissimilar films on a massive substrate, we have successively $\eta_{so}(\text{Al}) = 0.161$, $\eta_{tr} = 0.965$, $\varepsilon_{tr} = 0.857$. Hence, $E_{tr} = 12.85$ keV, $R'(\text{Au}) = 217$ nm, $\eta'(\text{Au}) = 0.491$, $\eta'(\text{Si}) = 0.176$, $\eta'_{sf} = 0.3$, $\varepsilon'_{sf} = 0.676$, $F'_{sf} = 0.73$, finally $I'_{sf} = 0.913$. Here, the error is 4.7%, since the experimental value of the signal is $I'_{sf} = 0.87$.

## 4. Discussion of the results

The coefficients $\eta_{sf}$ and signals $I_{sf}$ calculated by the formulas given above for the $S_1$ system, as well as the coefficients $\eta'_{sf}$ and signals $I'_{sf}$ for the $S_2$ system are shown in Figs 5 and 6. For the $S_1$ structure, 'the Au film ($d_1 = 10.8$ nm) on a Si substrate' is a massive Au target for primary electrons with energy $E_B$ ranging from 1 to 5 keV (Fig. 3a). Therefore, the coefficient $\eta_0(\text{Au})$ in this energy range increases according to (3), which is shown by the characteristic $\eta_{sf}$ curves in Fig. 5.

A similar increase in $\eta_{sf}$ for a 19.9 nm thick Au film is observed up to energies $E_B \approx 7$ keV. However, an Al film with a thickness of $t = 150$ nm is a massive target in the energy range from 1 to 5 keV (Fig. 3a). Therefore, according to formula (3), $\eta_s(\text{Al})$ decreases with increasing $E_B$. When the energy $E_B$ exceeds 5 and 7 keV, an increasing number of primary electrons are reflected from the $S_1$ system (Au/Si) rather than from the Au film, and the dependence $\eta_{sf} = f(E_B)$ is characterized by a decreasing function (6) (see Fig. 5). However, for the $S_2$ system, the opposite situation is observed — the initial growth of $\eta'_{sf}$ is replaced by a decline, the maximum value of $\eta'_{sf}$ being an individual characteristic achieved at certain values of the energy $E_B$. As a result, we have an intersection of graphs for $\eta_{sf}(E_B)$ and $\eta'_{sf}(E_B)$ and their corresponding inversion. For example, for a 10.8 nm

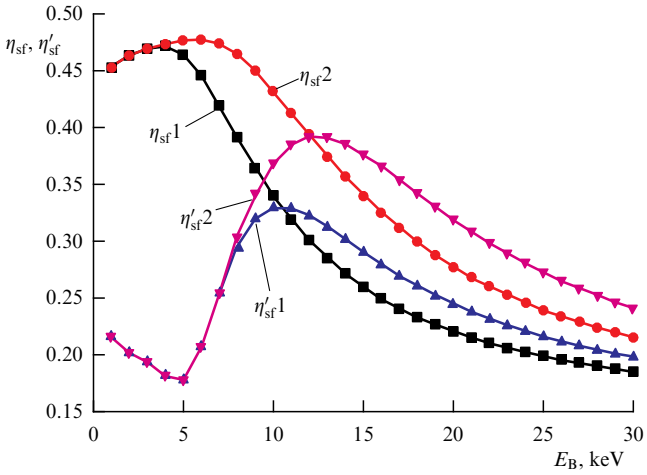


**Figure 5.** Dependences of reflection coefficients $\eta_{sf}$ and $\eta'_{sf}$ on energy of irradiating electrons for composite systems $S_1$ and $S_2$, respectively (shown in Fig. 4).

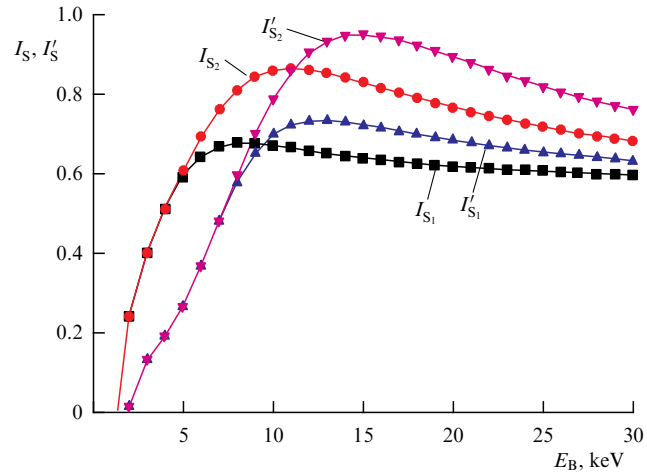


**Figure 6.** Dependences of calculated values of signals $I_S$ and $I'_S$ from semiconductor BSE detectors for systems $S_1$ and $S_2$ on energy $E_B$ of irradiating electrons: $I_{S_1}$ for $t = 0$, $d = 10.8$ nm, $I_{S_2}$ for $t = 0$, $d = 19.9$ nm, as well as $I'_{S_1}$ for $t = 150$ nm, $d = 10.8$ nm, $I'_{S_2}$ for $t = 150$ nm, $d = 19.9$ nm.

thick An film, the intersection of the $\eta_{sf}(E_B)$ and $\eta'_{sf}(E_B)$ graphs is observed at $E_B \approx 11$ keV. Up to $E_B = 11$ keV and higher, $\eta_{sf} > \eta'_{sf}$ and $\eta_{sf} < \eta'_{sf}$, respectively. At such energies, there occurs contrast inversion of the BSE images similar to those shown in Fig. 2. This fact is an indisputable proof of an increase in the BSE coefficient under certain conditions. To exclude the ambiguity of this statement, we calculated the $I_S$ signal from the structure in question as a function of $E_B$, $d$, and $t$ for the $S_1$ and $S_2$ systems. The calculations were made using formulas (1) and (2), i.e., taking into account the contribution of not only the BSE coefficients $\eta_{sf}$, but also their average reflected energy $\varepsilon_{sf}$ and the detector response function $F_{sf}$ to the signal. The calculation results are shown in Fig. 6. The signals $I_S$ and $I'_S$ for the systems $S_1$ and $S_2$, respectively, are limited along the $E_B$ axis by the $E_{th}$ value (0.75 keV $< E_{th} <$ 2.5 keV), initially increase, and reach a maximum, after which they tend to a constant value with a tendency to slowly decrease. As in the case of the regularities for $\eta_{sf}(E_B)$, and $\eta'_{sf}(E_B)$ shown in Fig. 5, we again observe an inversion of the graphs for $I_S$ and $I'_S$. The full expanded

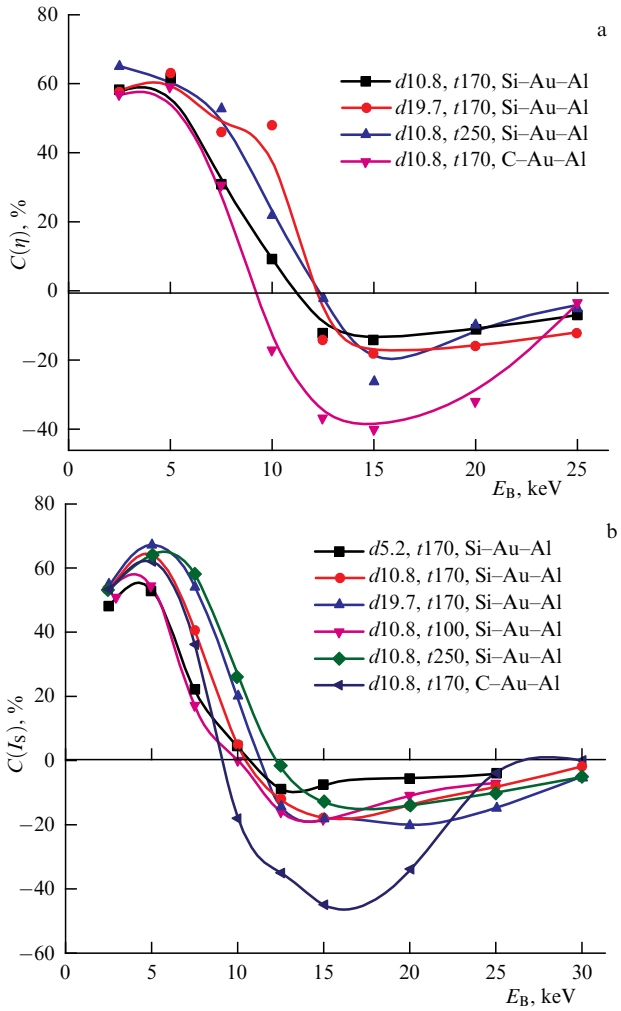


**Figure 7.** Contrast of images of multilayer nanostructures as a function of accelerating voltage of an SEM: (a) $C(\eta)$ and (b) $C(I_S)$ with parameters $d$ and $t$ indicated in the figures.

formula (13) includes several increasing and several decreasing exponentials. Their combination leads to the presence of a maximum in the graphs, $I_S = f(E_B)$.

The decisive and determining factor of the image contrast inversion is the increase in the number of reflected electrons in the sections hidden by the surface film. This conclusion is confirmed by the results of calculating the contrast of the images shown in Fig. 7. Contrast $C$ was estimated by the relations:

$$C(I_S) = \frac{I_{S_1} - I_{S_2}}{I_{S_1}} \times 100\%\,, \qquad (14)$$

$$C(\eta) = \frac{\eta_{sf} - \eta'_{sf}}{\eta_{sf}} \times 100\%\,.$$

The contrast was calculated for various combinations of the film compositions and thicknesses $d$ and $t$ and for various substrate materials. Massive samples of silicon and carbon were taken as substrates. The film material consisted of aluminum, gold, and nickel with different thicknesses $d$ and $t$. For all combinations, a general trend is observed, shown in Fig. 7, where the calculated values of contrast for a number of samples are given as an example. A higher contrast is noticeable for a substrate made of a low-$Z$ material, for example, carbon compared to silicon. The contrast increases with the growth of the atomic number $Z$ of the film material on the substrate and the thickness $d$ of this film (higher contrast on Au samples compared to Ni). An extreme dependence on the material and thickness $t$ of the upper film is found.

The presented results demonstrate that the estimates of the image contrast using both formulas (14) give consistent values. This confirms the priority contribution of the BSE coefficients to the contrast characteristics.

## 5. Conclusions

We solved the direct and inverse problems of establishing the relationship between the detected signal of backscattered electrons from multilayer nanostructures in an SEM and the parameters of a massive substrate and composite films on its surface. The problem was solved using refined formulas for the coefficient of the backscattered electrons and their energy, for the most probable energy of transmission electrons, and for the hardware function of the measuring device. These formulas can serve as a reference material for SEM users. The proposed algorithm for finding thicknesses of subsurface local films or any bulk inhomogeneous inclusions in the matrix of an optically opaque sample allows the depths and thicknesses to be determined with an error of up to 10%. For example, for a buried film 5 nm-thick, the measurement error is $\pm 0.5$ nm with a lateral resolution of nm. For nondestructive methods of diagnostics and visualization of local nanostructures, such results are the most accurate.

The effect of increasing the BSE coefficient is inherent only in layered nanosystems containing a substrate and a cover film of light elements (small $Z$) and an intermediate layer of a material with a higher atomic number $Z$.

Topics such as the efficiency of such an electron-multiplying system with an oblique incidence of primary electrons, finding the optimal composition and thickness of films, and the energy range of the amplified electron flow require further additional research, as does the problem of the possible application of the effect in modern nanotechnology.

## References

1. Reimer L *Scanning Electron Microscopy. Physics of Image Formation and Microanalysis* (Springer Series in Optical Sciences, Vol. 45) 2nd ed. (Berlin: Springer, 1998) https://doi.org/10.1007/978-3-540-38967-5
2. Goldstein J I et al. *Scanning Electron Microscopy and X-Ray Microanalysis* (New York: Springer, 1981) https://doi.org/10.1007/978-1-4613-3273-2; Translated into Russian: *Rastrovaya Elektronnaya Mikroskopiya i Rentgenovskii Mikroanaliz* (Moscow: Mir, 1984)
3. DeNee P B, in *Scanning Electron Microscopy* Vol. 1 (Ed. O Johari) (AMF O'Hare (Chicago), IL: Scanning Electron Microscopy, Inc., 1978) p. 479
4. Dapor M *Phys. Rev. B* **43** 10118 (1991)
5. Dapor M *Phys. Rev. B* **48** 3003 (1993)
6. Assa'd A M D *Appl. Phys. A* **124** 699 (2018)
7. Afanas'ev V P, Kaplya P S, Kostanovskii I A *Poverkhnost' Rentgen. Sinkhrotron. Neitron. Issled.* (2) 30 (2013)
8. Mikheev N N *Poverkhnost' Rentgen. Sinkhrotron. Neitron. Issled.* (12) 70 (2020)
9. Zaitsev S V, Kupreenko S Yu, Rau E I, Tatarintsev A A *Instrum. Exp. Tech.* **58** 757 (2015); *Prib. Tekh. Eksp.* (6) 51 (2015)
10. Niedrig H *Optica Acta Int. J. Opt.* **24** 679 (1977)
11. Zaitsev S V, Zykova E Yu, Rau E I, Tatarintsev A A, Kiselevskii V A *Instrum. Exp. Tech.* **66** 1058 (2023); *Prib. Tekh. Eksp.* (6) 167 (2023)

12. Jackson A R et al. *Surf. Interface Analysis* **25** (5) 341 (1997)
13. Karavaev M B et al. *Semiconductors* **51** 54 (2017); *Fiz. Tekh. Poluprovodn.* **51** (1) 56 (2017)
14. August H-J, Wernisch J *J. Microscopy* **157** (2) 247 (1990)
15. Rau E I, Zaitsev S V, Karaulov V Yu *Tech. Phys. Lett.* **48** (23) 18 (2022) http://dx.doi.org/10.21883/TPL.2022.12.54939.19361; *Pis'ma Zh. Tekh. Fiz.* **48** (23) 22 (2022) http://dx.doi.org/10.21883/PJTF.2022.23.53947.19361
16. Fitting H-J et al. *J. Electron Spectrosc. Related Phenom.* **159** (1-3) 46 (2007)
17. Aristov V V, Dremova N N, Likharev S K, Rau E I *Elektron. Promyshlennost'* (2) 44 (1990)
18. Aristov V V et al. *Acta Phys. Polon. A* **83** (1) 81 (1993)
19. Hejna J *Scanning* **14** 256 (1992)
20. Orlikovsky N A, Rau E I *Bull. Russ. Acad. Sci. Phys.* **75** 1234 (2011); *Izv. Ross. Akad. Nauk Ser. Fiz.* **75** 1305 (2011)
21. Kowoll T et al. *Scanning* 4907457 (2017) https://doi.org/10.1155/2017/4907457
22. Lutter F et al. *Nucl. Instrum. Meth. Phys. Res. B* **500–501** 10 (2021)
23. Zschech E, Yun W, Schneider G *Appl. Phys. A* **92** 423 (2008)
24. Zegenhagen J, in *Synchrotron Light Sources and Free-Electron Lasers. Accelerator Physics, Instrumentation and Science Applications* (Eds E J Jaeschke et al.) 2nd ed. (Cham: Springer, 2020) p. 1825, https://doi.org/10.1007/978-3-030-23201-6_66
25. Matveevskii K et al. *J. Appl. Crystallogr.* **57** 1288 (2024)
26. Kim H et al. *J. Electron Microsc.* **59** (5) 379 (2010)
27. Sánchez E, Torres Deluigi M, Castellano G *Microscopy Microanalysis* **18** 1355 (2012)
28. Wilson D J, Curzon A E *Thin Solid Films* **165** 217 (1988)
29. Arnal F, Verdier P, Vincensini P *C. R. Acad. Sci.* **268** 1526 (1969)
30. Hunger H J, Küchler L *Phys. Status Solidi A* **56** (1) K45 (1979)
31. Staub P-F *J. Phys. D* **27** 1533 (1994)
32. Bronstein I M, Freiman B S *Vtorichnaya Elektronnaya Emissiya* (Secondary Electron Emission) (Moscow: Nauka, 1969)
33. Joy D C *Scanning* **17** (5) 270 (1995)
34. Frank L et al. *Microchim. Acta* **132** 179 (2000)
35. Fitting H-J *J. Electron Spectrosc. Related Phenom.* **136** (3) 265 (2004)
36. Fitting H-J *J. Phys. D* **8** 1480 (1975)
37. Cosslett V E, Thomas R N *Br. J. Appl. Phys.* **15** 883 (1964) https://doi.org/10.1088/0508-3443/15/8/303
38. August H-J, Wernisch J *Ultramicroscopy* **32** (2) 113 (1990)
39. Reimer L, Senkel R *Optik* **98** (3) 85 (1995)